DOI: 10.1002/ejic.201001069

Photoactive Europium Hybrids of β-Diketone-Modified Polysilsesquioxane Bridge Linking Si–O–B(Ti)–O Xerogels

Chang Wang,[a] Bing Yan,*[a] Jin-Liang Liu,[a] and Lei Guo[a]

Keywords: Organic-inorganic hybrid composites / Europium / Luminescence / Composite xerogels

Polysilsesquioxane bridges are obtained through the single modification of 3-(triethoxysilyl)propyl isocyanate (TEPIC) by two β-diketone ligands [thenoyltrifluoroacetylacetone (TTA) and trifluoroacetylacetone (TA)], which behave as linkages between the europium ion and composite host Si–O–M (M = B or Ti) xerogels by controlling the hydrolysis rate of the alkoxy compounds (tetraethyl orthosilicate, titanium butoxide and tributyl borate). Subsequently, luminescent europium hybrid xerogels are assembled and characterized by NMR, Fourier transform infrared (FTIR), ultraviolet absorption and ultraviolet/visible diffuse reflection spectroscopy, X-ray diffraction (XRD), thermogravimetric analysis (TGA), scanning electron microscopy (SEM), and photoluminescence spectroscopy through which the decay times (τ) and quantum efficiency (η) can be determined. These results reveal that the lanthanide complexes have been covalently immobilized into the composite inorganic xerogels and the obtained hybrids have the excellent ability of light absorption and emission. The hybrids with composite Si–O–B xerogels possess the matched photoluminescent properties (red emission intensity, lifetimes, and quantum efficiency) as the pure silica oxygen network, both of which show a superior luminescence performance than the hybrids with composite Si–O–Ti xerogels. Besides, the single modification of TTA is favorable for the luminescence of the hybrid xerogels.

Introduction

It has long been recognized that trivalent lanthanide ions have excellent optical properties such as large Stokes shifts, high luminescence quantum efficiency, and sharp emission spectra etc.[1] However, lanthanide ions have not been widely applied in luminescent materials for their poor light absorption ability. The f–f transitions of lanthanide ions belong to the spin forbidden ones, so it is difficult to generate efficient luminescence emission by direct excitation. Lanthanide complexes are much more outstanding than simple lanthanide ions with respect to light emission because of the so-called "antenna effect";[2] therefore, they offer potential applications in many fields of optical amplification, organic light-emitting diodes, tunable solid-state lasers, phosphors, and luminescent sensors.[3] However, the practical application of these materials in optical devices is limited to a large extent by their poor stability under high temperature, high pressure, or moisture conditions and low mechanical strength.[4]

The proposal of new concept "organic/inorganic hybrid materials" brings lanthanide luminescent materials new development opportunities.[5] The combination of organic and inorganic components at a molecular or a nanometer level brings together the integration of certain strong points of organic compounds (easy processing with conventional techniques, elasticity, and organic functionalities) with the advantages of the inorganic composition (hardness, thermal and chemical stability).[6] Similarly, luminescent lanthanide hybrid materials obtained by grafting lanthanide complexes onto some matrices, such as silica-based materials,[7] polymers,[8] or liquid crystals,[9] can exhibit excellent optical properties and good thermal and compressive stabilities[10] relative to the pure lanthanide complexes. According to the different force acting between the two phases, organic–inorganic hybrid materials are divided into two major classes. There are weak interactions (such as hydrogen bonding, van der Waals forces, or weak static effects) between the organic and inorganic phases,[11] so there are many problems such as clustering of the emitters, inhomogeneous dispersion of the components, or leaching of the dopants. By strong chemical bonds, such as covalent, iono-covalent, or Lewis acid base bonds,[12] grafting of the complexes onto sol–gel-derived host materials produce the second class of hybrid materials.[13] The latter class overcomes the disadvantages of the former class, as it encourages homogeneity and avoids the self-quenching of lanthanide ions, which results in increasing concentrations.

Luminescent lanthanide hybrid materials based on silicate systems have been quite well developed. Carlos and Binnemans both have reviewed the topic.[14] Our research team has done extensive work on covalently grafting the ligands to the inorganic networks, in which the lanthanide

[a] Department of Chemistry, Tongji University,
Siping Road 1239, Shanghai 200092, China
Fax: +86-21-65982287
E-mail: byan@tongji.edu.cn

Supporting information for this article is available on the WWW under http://dx.doi.org/10.1002/ejic.201001069.

complexes luminescence centers are bonded with a siloxane matrix through Si–O linkages. We have successfully realized six paths for the construction of the functional silylated precursors. In addition, after modification, we have assembled the above modified bridge ligands with lanthanide ions and tetraethoxysilane (TEOS) to compose hybrid systems with covalent bonds, and we obtained a series of stable and efficient molecular hybrid materials for use in optical areas.[15–17] However, it is a pity that other elements have hardly, even never, been introduced into the host networks of organic–inorganic hybrid materials.[18] Titanium and boron have attracted the attention of our team owing to their interesting properties. Titanium is an exotic metal, which can be applied to photocatalytic and energy conversion,[19] meanwhile, boron has a strong bonding ability, in its elemental form and in compounds with complex structures. Therefore, the introduction of titanium or boron into organic–inorganic hybrid materials will probably improve these materials and thus generate new materials with more advanced properties. Currently, as far as we know, reports on lanthanide complexes grafted onto titanium gel and boron gel to host a network of hybrid materials are few.[18]

In this paper, on the basis of our previous work on the modification of β-diketone for the construction of hybrids,[16,17b,18a] we synthesize a series of luminescent organic–inorganic hybrid xerogels with a composite host using titanium/boron instead of partial silicate covalently bonded to form Si–O–Ti or Si–O-B networks through a sol–gel process. For comparison, some luminescent organic–inorganic hybrids based on silicate systems are also prepared. Moreover, the luminescence properties, microstructure, and thermal stabilities of these materials are analyzed in detail.

Results and Discussion

The synthesis for the silylated precursors (TTASi, TTASi′, TAASi) through the extraction of the methylene group and the predicted structure of the hybrid materials are shown in Figures 1 and S1. Here it should be noted that single modification of a hydrogen atom of the methylene is important for two reasons: the first is because of the decrease in the steric hindrance effect from the large silylated groups and the second is because the unsymmetrical structure is able to achieve an effective photoactivity.[20] For comparison, we also selectively prepared hybrids with double modification of TTA (TTASi′). The bifunctional β-diketone molecular bridge not only has the capability of coordinating to lanthanide ions but can also form covalently bonded Si–O networks after the cohydrolysis and copolycondensation with TEOS (TBB, TBNT) through their alkoxy groups. These kinds of hybrid materials belong to a complicated huge molecular network. To date, the structural characterization of these non-crystalline hybrid materials remains a challenge. However, we can predict the main composition and coordination effect of these hybrids by knowledge of lanthanide coordination chemistry principles and the behavior of the functional groups of the organic unit. The modified β-diketone ligands (TTASi, TTASi′, TASi) still possess two chelated oxygen atoms, and from the molar ratio 1:3 of β-diketone ligands to Eu^{3+}, it can seen that six coordination positions are occupied by three of these ligands. Water molecules occupy the remaining positions to form an eight-coordination number structure for common RE^{3+} species. These predictions have also been confirmed by infrared spectroscopy.

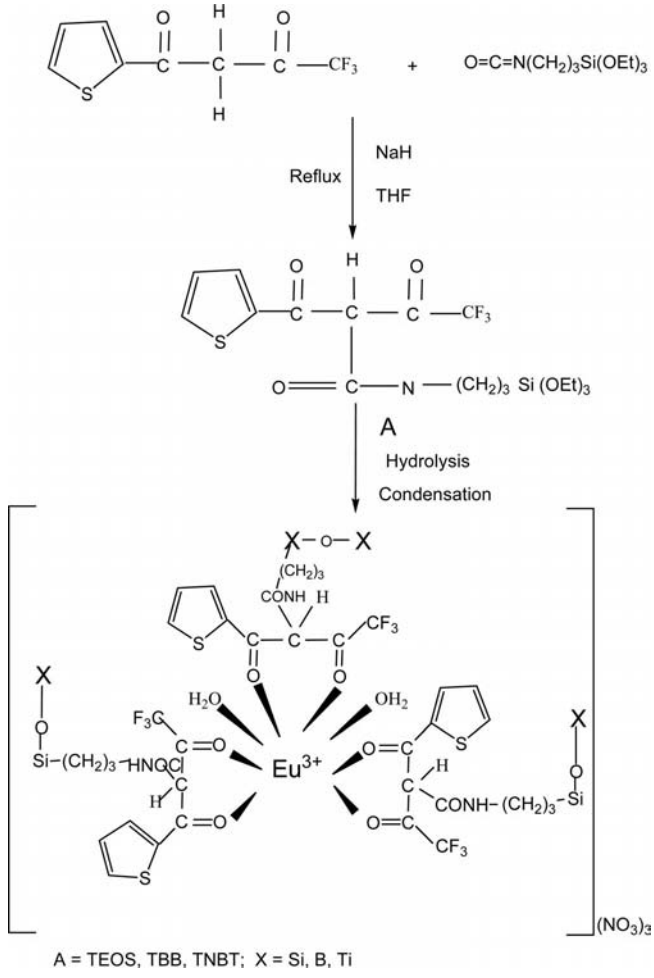

Figure 1. Selected scheme of the synthesis processes and predicted structure of europium-centered covalently bonded hybrids Eu-TTASi-X (B = Si, B, Ti).

The IR spectra of the ligand (TTA, TA), the coupling agents (TEPIC), and the precursors (TTASi, TASi, TTASi′) are shown in Figures S2 and S3. In Figure S3, an example for the TTASi′ system is shown. It can be observed that CH_2– stretching vibration peak of TTA at 3110 cm^{-1} is replaced by a strong broad band centered at 2956 cm^{-1}, which derives from the three methylene groups of TEPIC. Moreover, in the spectrum for TTASi′ (Figure S3), the vibration peaks at 1274 cm^{-1} and 1085 cm^{-1} are assigned to ν(C-Si) and ν(Si-O) stretching vibration absorption bands, respectively, and the band centered at 3340 cm^{-1} corresponds to the stretching vibration of the grafted NH– group. The bending vibration [δ(NH), 1527 cm^{-1}] further proves the

formation of amide groups. New bands at 1695 and 1625 cm^{-1} formed in the spectrum for TTASi′, attributed to the C=O absorption bands of TEPIC,[21] and the disappearance of the vibration peak (N=C=O) at 2274 cm^{-1}, prove that TEPIC has been grafted onto the β-diketone ligand TTA.[22] Figure S2 shows the similar features for the TTASi and TASi series.

Figure 2 shows selected ultraviolet absorption spectra of TTA (TA) and TTASi (TASi). In Figure 2A, we can see a slight blueshift in the major π–π* electronic transition for the thenoyl ring on going from TTA to TTASi (from 266 to 258 nm) and a redshift (from 324 to 338 nm) for the conjugated diketones groups occur, which indicates that the electron distribution of the conjugated system has changed after TEPIC is introduced into the β-diketone TTA. For Figure 2B, the redshift from 278 to 285 nm appears, which suggests that TA is grafted by TEPIC. Further, it can be seen that there is a large overlap between the absorption bands of the precursors (TTASi, TASi) and the excitation bands of the hybrid gels (will be shown in afterwards), which suggests that the TTA or TA groups can sensitize the central Eu^{3+} ion in the hybrid material efficiently, namely causing the antenna effect. Consequently, we can draw the conclusion that intramolecular energy transfer occurs between the β-diketone modified unit and the Eu^{3+} ion in the hybrid materials; this conclusion will be further proven by the emission spectra of the corresponding materials. Figure S3 shows similar results for the ultraviolet absorption spectra of the TTASi′ series.

Figure 3A shows selected FTIR spectra of three binary hybrid xerogels with the TASi linkage with different inorganic compositions and the pure europium complex of TA. The high-frequency bands in the range 3400–1600 cm^{-1} can be ascribed to the stretching vibration of the O–H group.[23] The absorption peaks within the range 1050–1350 cm^{-1} originate from the stretching vibrations of the M–O–M and M–O–M′ bonds (M and M′ = Si, B, Ti).[24] Unfortunately, the distinction between M–O–M and M–O–M′ is not clearly shown. Furthermore, the peaks at about 1650 and 1560 cm^{-1} originate from the CONH– group of the modified organic ligands.[25] The apparent band at 1380 cm^{-1} indicates the characteristics of NO_3^-. In Figure 3B the IR spectra of binary hybrid gels with different composite hosts

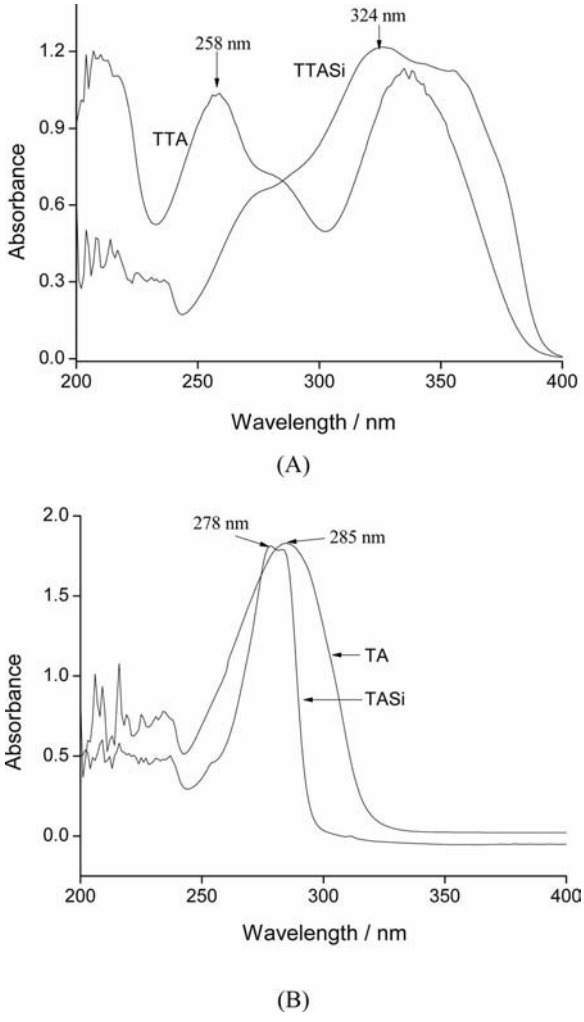

Figure 2. Selected UV/Vis absorption spectra of the single-modified precursor and ligands (A) TTA series, (B) TA series.

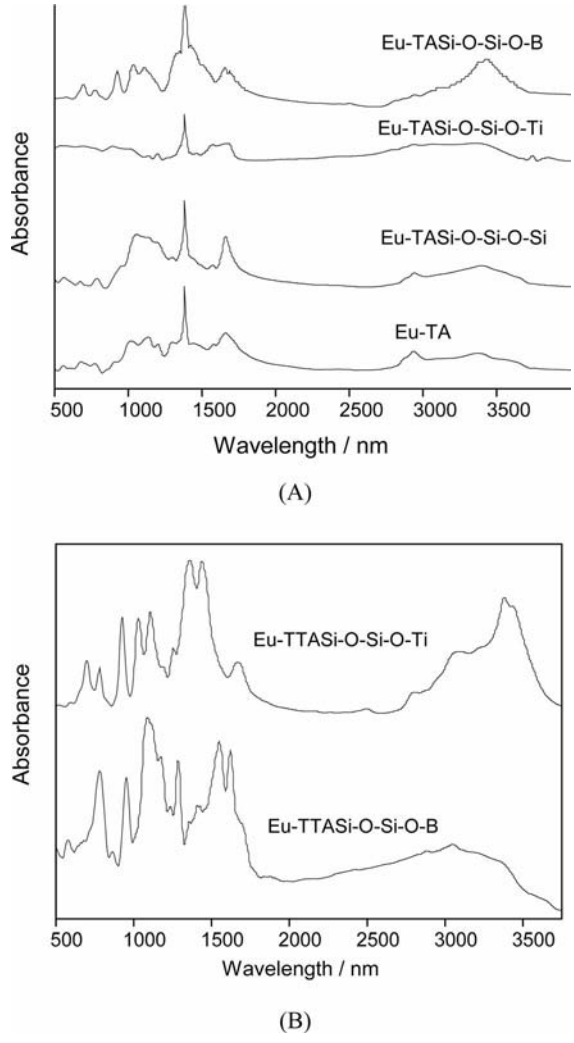

Figure 3. Selected FTIR spectra of europium-centered hybrids with the single-modified precursor (A) TAA series, (B) TTA series.

is compared, which also shows a similar character to that of the TA series. No apparent distinction can be observed among the different composite M–O–M′ frameworks, which suggests a homogeneous sol–gel process to form the uniform hybrid systems.

Figure S4 show the selected room-temperature X-ray diffraction patterns of the europium hybrid xerogels with single-modified linkage TTASi and TASi from 10 to 70°. There are no crystalline regions in these hybrid materials, which is due to the presence of an organic moiety in the host inorganic framework. From Figure S4, it can be seen that the diffraction curves show similar broad peaks, with angle 2θ centered at about 21°, which is characteristic of amorphous silica, titanium, and boron materials. This may be attributed to the coherent diffraction of the amorphous inorganic backbone of the hybrids or a periodic distance because of the organic moiety. In addition, there are no measurable amounts of phases corresponding to the pure organic compound or free RE nitrate in these hybrid materials, which proves, to a certain extent, the formation of the true covalent-bonded hybrid xerogels.

Differential thermogravimetric analyses (TGA) were performed on part of the obtained materials in an N_2 atmosphere. Figure 4 compares the selective TG traces of the europium hybrid gels with the TTASi linkage with different host compositions (Eu–TTASi–O–Si–O–M, M = Si, B, Ti). These three samples show similar trends in weight loss and three main degradation steps. There is slight weight loss (approximately 4% for Eu–TTASi–O–Si–O–B, 6% Eu–TTASi–O–Si–O–Ti, 10% for Eu–TTASi–O–Si) in the first step from 150 to 200 °C with a heat flow of about 170 °C. This step may be ascribed to desorption of adsorbed water and residual solvent DMF, which is an endothermic process, as seen according to the DSC curves (not given). The second mass loss (about 17% for Eu–TTASi–O–Si, 9% for Eu–TTASi–O–Si–O–Ti, 8% for Eu–TTASi–O–Si–O–B) between 200 and 290 °C with a heat flow of about 246 °C (as the fastest speed) could be attributed to the preliminary decomposition of the TTA organic ingredients. As seen from the TG curves, all the materials exhibit the biggest weight loss in the third step (about 20% for Eu–TTASi–O–Si, 12% for Eu–TTASi–O–Si–O–Ti, 28% for Eu–TTASi–O–Si–O–B) beyond 290 °C, which can be assigned to further decomposition of the TTA organic ingredients and the demolition of the inorganic frameworks. As is clearly observed in the whole process, the thermal stabilities of all these materials are improved relative to the organic ligand. From their mass loss curves; we can conclude that the silica and titanium/boron network (Si–O–Ti/B) is a better inorganic matrix than the silica and silica network (Si–O–Si), which is the result we wanted to achieve in these experiments. Figure S5 shows a comparison between the representative europium hybrid gel Eu–TASi–O–Si–B and its pure complex Eu–TA. In general, there is one main result caused by introduction of the inorganic networks to the organic complex: the thermal stabilities of all these hybrids are improved relative to that of the pure complex Eu–TA. The inorganic component provides a protective barrier against thermal degradation of the organic species. Further, Figure S5 also reveals that the thermal stability caused by different inorganic host networks differs.

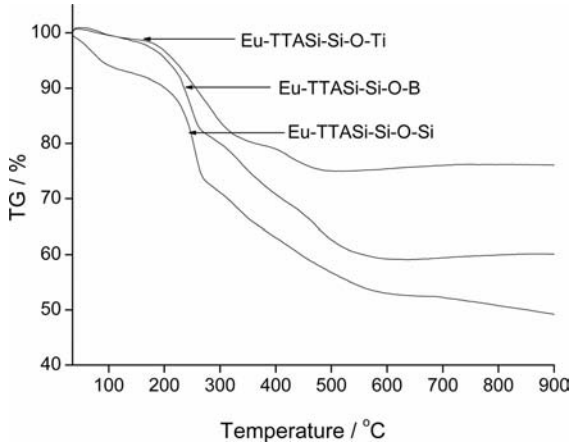

Figure 4. Selected thermogravimetry trace (TG) of the hybrid gels Eu–TTASi–O–Si, Eu–TTASi–O–Si–O–B, and Eu–TTASi–O–Si–O–Ti.

Figure 5 displays the scanning electron micrographs of the representative lanthanide hybrid xerogels. These micrographs demonstrate that homogeneous materials are obtained with covalent bonds connecting the organic β-diketone (TTA) group to the inorganic networks. The inorganic and organic phases can exhibit their distinct properties together in the hybrid xerogels compared to the hybrids with doped lanthanide complexes, which generally experience the phase separation phenomena.[26] Moreover, on the surface of these materials, there are many granules, which are residual solvent or precursor material. It is interesting that the regular and uniform dendritic striped microstructure appears on the surface of these materials. In the hydrolysis

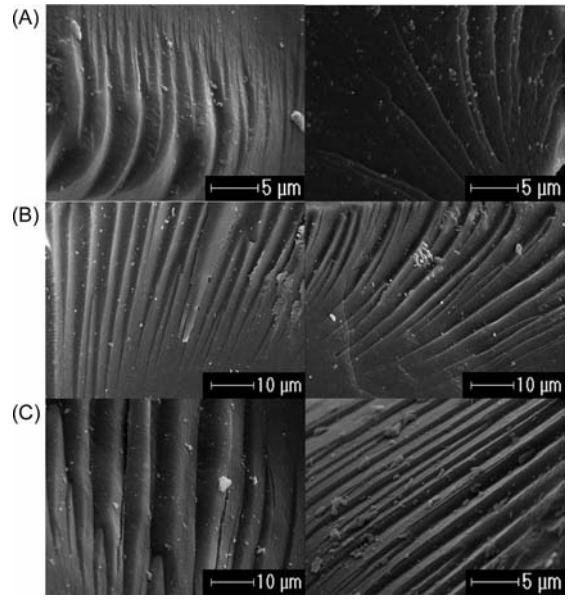

Figure 5. SEM images of the hybrid materials (A) Eu–TTASi–O–Si–O–B, (B) Eu–TTASi–O–Si–O–Ti, (C) phen–Eu–TTASi–O–Si–O–Ti).

and condensation processes of silica and titanium/boron, the coordination reaction acts together with the sol–gel process, so it is seen from the final structure and morphology that there is a homogeneous bulk trunk-type or tree-type striped microstructure on the surfaces of each of these hybrid materials. We were interested in the unusual phenomenon: there are many holes with different diameter sizes on the surface of the hybrid xerogel shown in Figure 5A. We conjecture that there are two reasons for these holes: one is the evaporation of the solvent (THF) through ageing and the other is the largely different hydrolysis rate between tetraethyl orthosilicate and tributyl borate. Moreover, as seen from Figure 5C, ternary complexes show a similar microstructure, which reveals that the introduction of the second ligand phen hardly affects the microstructure in these hybrids.

All the materials were studied by diffuse reflectance spectroscopy to investigate the influence caused by the different inorganic networks. The corresponding spectra are shown in Figures S6 and S7. It is observed that all of the materials exhibit a similar broad absorption band in the UV/Vis range (200–400 nm), which corresponds to a transition from the ground state of the organic ligand to the first excited state (S0 → S1). It is more specifically attributed to a π→π* transition of the TTA or TA. According to Dexter's exchange energy transfer theory, which states that [27] the luminescence intensity of the hybrid material rests with the matching degree between the triplet-state energy of ligand and the excited-state energy of lanthanide ion, we can primarily predict that the energy level difference between TTA or TA and Eu^{3+} is such that the organic ligand can absorb abundant energy in the UV/Vis range and transfer it to the corresponding lanthanide ion. So we can conclude that the final hybrid materials can be expected to exhibit excellent luminescence properties, which is proven by the fluorescence spectra analysis.

We have investigated the luminescence behavior of all the obtained lanthanide hybrids at room temperature. Figure 6 shows selected excitation spectra of the europium hybrids with two β-diketone-functionalized linkages (TASi and TTA series), which were obtained by monitoring the emission of the Eu^{3+} ions at 613 nm. It can be seen that all these materials have similar excitation spectra, which are dominated by broad bands from 220 to 400 nm with a maximum peak at about 360 nm in the ultraviolet region. These bands originate from the β-diketone modified Si–O–M (M = Si, B, Ti) host with conjugated C=O groups. For the TASi series, the weak sharp excitation peak for the f–f transition of Eu^{3+} can be found at around 396 nm, while it cannot be found in the excitation spectra of TTASi series. It can therefore be predicted that the TTASi series may be expected to have more effective luminescence than the TASi series. The broad excitation bands are favorable for energy transfer and luminescence of Eu^{3+}. In addition, the hybrids with the TTASi linkage show a similar excitation band to that for the pure europium complex of the TTA ligand, which suggests that modification of TTA does not have a large influence on energy absorption. It is interesting to note that the hybrids with the composite host Si–O–B show a stronger excitation intensity than that for Si–O–Ti, even stronger than that of the pure Si-O-Si host. Therefore Si–O–B may be a candidate host for the luminescence for the europium hybrids.

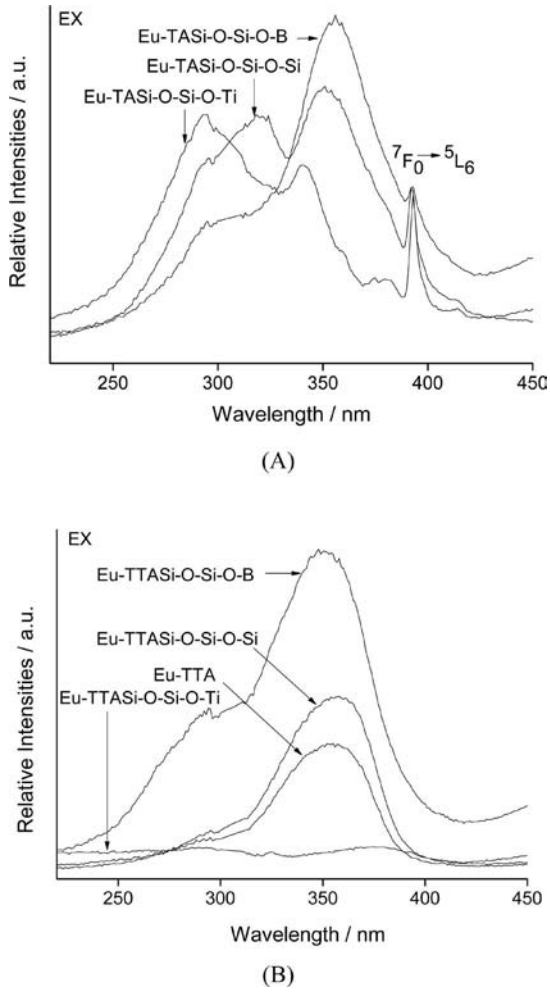

Figure 6. Excitation spectra of the europium hybrids with different Si–O–M (M = Si, B, Ti) hosts with TASi and TTASi linkages.

The corresponding emission spectra are shown in Figure 7. We can observe strong red luminescence, which reveals that effective energy transfer takes place, and conjugated systems are formed between the ligands and the central Eu^{3+} ions in these hybrids materials. The emission bands of these samples in Figure 7A (Eu–TASi–O–Si–O–B, Eu–TASi–O–Si–O–Si, Eu–TASi–O–Si–O–Ti) are assigned to the $^5D_0 \rightarrow {}^7F_0$, $^5D_0 \rightarrow {}^7F_1$, $^5D_0 \rightarrow {}^7F_2$, and $^5D_0 \rightarrow {}^7F_3$ transitions at 578 (577, 579), 590 (589, 590), 615 (614, 613) and 650 (650, 652) nm, respectively, under excitation at a wavelength of 360 nm. By comparing the spectra, it can be seen that the luminescent intensity of Eu–TASi–O–Si–O–B is slightly stronger than that of Eu–TASi–O–Si–O–Si and Eu–TASi–O–Si–O–Ti (Eu–TASi–O–Si–O–Ti possesses the weakest intensity), which indicates that Eu–TASi–O–Si–O–B is a good host for the luminescence of Eu^{3+} as well as

pure Eu–TASi–O–Si–O–Si systems. This can be interpreted that substitution of Si by B still maintains a similar chemical environment of the whole hybrid host system, as B and Si are located diagonally as elements of the periodic table of elements and show similar features and chemical behavior. This point can be verified from the sol–gel processes of their alkoxy compounds.[28] Further, it can be observed that there exists some bands in the short wavelength region (450–550 nm), which can be ascribed to the emission of the TA-modified Si–O–M framework. It is interesting to note that the intensities of these three systems show the reverse order to those of the $^5D_0 \rightarrow {}^7F_2$ transition of Eu^{3+}, which suggests a different energy transfer between the TA-modified Si–O–M framework and central Eu^{3+}. Figure 7B presents the three hybrid systems with the TTASi linkage, which shows similar results to those in Figure 7A. Moreover, a comparison of the luminescence intensity of these hybrids and that of the pure europium complex of the TTA ligand is made, which shows that the intensity of the Eu–TASi–O–Si–O–Ti hybrids is even lower than that of the pure complex.

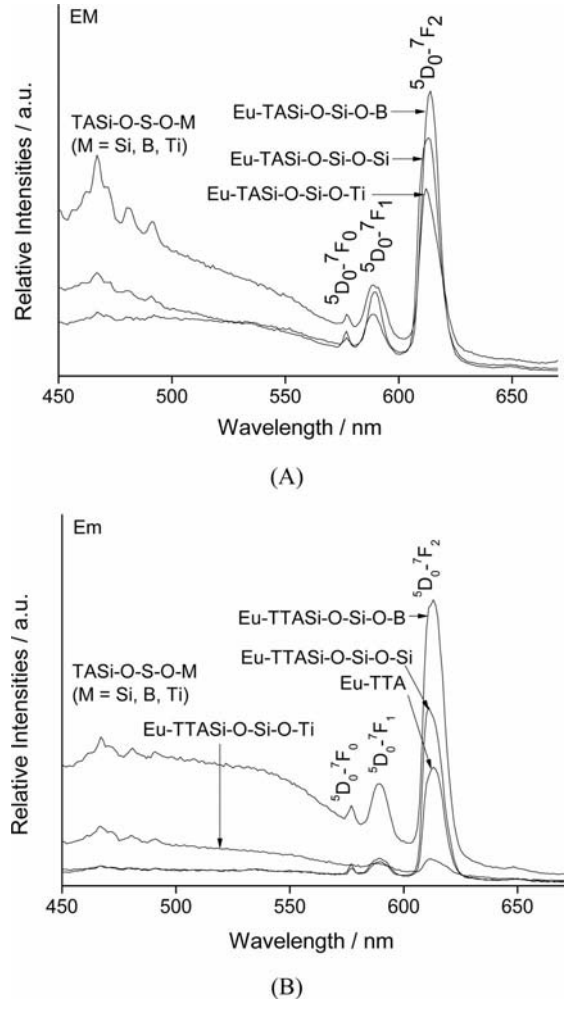

Figure 7. Emission spectra of the europium hybrids with different Si–O–M (M = Si, B, Ti) hosts with TASi and TTASi linkages.

In the emission spectra of these hybrids, among all the emission transitions, the most predominant transition is $^5D_0 \rightarrow {}^7F_2$ at about 615 nm, which corresponds to a typical electric dipole transition and strongly varies with the local symmetry of Eu^{3+}, while the $^5D_0 \rightarrow {}^7F_1$ transition corresponds to a parity-allowed magnetic dipole transition and is independent of the host material. Therefore, the emission spectra indicate that the Eu^{3+} site is situated in an environment without inversion symmetry, which reveals that effective energy transfer takes place from the precursors to the coordinated Eu^{3+} ions.[29] The asymmetric microenvironment will induce the polarization of Eu^{3+} because of the influence of the electric field of the ligand and the high probability of the electric dipole transition. The non-symmetry and the intensities of the electric dipole transition $^5D_0 \rightarrow {}^7F_2$ increases with an increase in the interaction of the rare earth complex with its local chemical environment, so the relative intensity ratio (I_{02}/I_{01}) of the $^5D_0 \rightarrow {}^7F_2$/$^5D_0 \rightarrow {}^7F_1$ transition has been widely used as an indicator of the Eu^{3+} site symmetry. The relative intensity ratio (I_{02}/I_{01}) of the $^5D_0 \rightarrow {}^7F_2$/$^5D_0 \rightarrow {}^7F_1$ transition for these europium hybrids are summarized in Table 1. The hybrid with a pure Si–O–Si host possesses the largest value, which indicates that Eu^{3+} is located in the most asymmetric environment. In addition, we also synthesized the hybrids with the TTASi′ linkage from double modification of TTA. The photoluminescence data are shown in Table 1. The relative intensity ratios (I_{02}/I_{01}) of Eu–TTASi–-O–Si–O–M are lower than those of Eu–TTASi–O–Si–O–M, which suggests that the double modification of the TTASi′ linkage improves the symmetry environment surrounding the Eu^{3+} ion within the hybrid systems.

Table 1. The luminescence quantum efficiencies and lifetimes of some hybrid xerogels.

Europium hybrids	I_{02}/I_{01}[a]	τ [μs][b]	A_{rad} [s^{-1}]	η [%]
Eu–TASi–O–Si–O–Si	6.5	460	409	18.8
Eu–TASi–O–Si–O–B	5.9	711	342	24.3
Eu–TASi–O–Si–O–Ti	4.4	426	291	12.4
Eu–TTASi–O–Si–O–Si	10.2	547	732	40.1
Eu–TTASi–O–Si–O–B	6.6	936	417	39.9
Eu–TTASi–O-Si–O–Ti	5.1	448	342	14.3
Eu–TTASi′–O-Si–O–Si	8.6	632	514	32.5
Eu–TTASi′–O-Si–O–B	6.0	708	377	26.7
Eu–TTASi′–O-Si–O–Ti	4.6	277	310	8.6

[a] The integrated intensity of the $^5D_0 \rightarrow {}^7F_J$ emission peaks. [b] The luminescence decay times of the $^5D_0 \rightarrow {}^7F_2$ transitions.

We measured the decay curves of these hybrid materials, and then we selectively determined the emission quantum efficiency (η) of the $^5D_0$ excited state from the emission spectra and the lifetime of the first excited level (τ, $^5D_0$) of Eu^{3+}. By assuming that only nonradiative and radiative processes occur in the depopulation of the $^5D_0$ excited state, we can define η as shown in Equation (1).[30]

$$\eta = A_r/(A_r + A_{nr}) \quad (1)$$

Here, A_r and A_{nr} are the radiative and nonradiative transition rates, respectively. By summing over the radiative

rates, A_{0J}, for each $^5D_0 \rightarrow {}^7F_J$ (J = 0–3) transition of Eu^{3+}, A_r can be obtained by Equation (2).

$$A_r = \Sigma A_{0J} = A_{00} + A_{01} + A_{02} + A_{03} \quad (2)$$

Here, we neglect the branching ratio for the $^5D_0 \rightarrow {}^7F_{4,5,6}$ transitions, whose corresponding emissions are not detected experimentally and whose influence can be ignored in the depopulation of the $^5D_0$ excited state.[30] It is well known that $^5D_0 \rightarrow {}^7F_1$ belongs to the isolated magnetic dipole transition, and it therefore has nothing to do with the chemical environment around the Eu^{3+} ion and can be considered as an internal reference for the whole spectrum. We can calculate A_{0J}, namely the experimental coefficient for spontaneous emissions according to Equation (3).[30]

$$A_{0J} = A_{00}\,(A_{0J}/I_{01})(\nu_{01}/\nu_{0J}) \quad (3)$$

A_{01} is the Einstein's coefficient of spontaneous emission between the $^5D_0$ and $^7F_1$ energy levels and can be considered to have a value of 14.65 s^{-1} in vacuo. When an average index of refraction n of 1.506 is considered, the value of A_{01} can be approximated to be 50 s^{-1} [$A_{01} = n^3 A_{01(vacuum)}$].[31] I_{0J} are the emission intensities of the $^5D_0 \rightarrow {}^7F_J$ transitions (J = 0–3), while υ_{0J} is the energy barrier and can be determined from the emission bands for the $^5D_0 \rightarrow {}^7F_J$ emission transitions of Eu^{3+}.[31] According to the literature,[31] the value of $A_{01} \approx 50\ s^{-1}$, the lifetimes ($\tau$), and the radiative ($A_r$) and nonradiative ($A_{nr}$) transition rates are related through Equation (4).

$$\tau_{exp} = (A_r + A_{nr})^{-1} \quad (4)$$

The quantum efficiencies of these hybrid materials are worked out and shown in Table 1. As can be seen from the equation to calculate the quantum efficiency (η), the value of η mainly depends on two factors: one is lifetime and the other is the I_{02}/I_{01} ratio (red/orange ratio). If the lifetimes and the red/orange ratios of certain hybrid materials are large, its quantum efficiency must be high. As shown in Table 1, the luminescence quantum efficiencies of the hybrids with a Si–O–B host show the highest values. In spite of their lower I_{02}/I_{01} ratios than those of the Si–O–Si host, their luminescence lifetimes are longer than those of the latter. For the hybrids with single modification linkages TASi and TTASi, the hybrids with TTASi linkage show the longer lifetimes and higher quantum efficiencies that those of the hybrids with the TASi linkage. This is not surprising as the thenoyl ring produces a larger conjugated system and TTA is a superior ligand for Eu^{3+} than TA. The Eu–TTASi′–O–Si–O–M hybrids possess the shorter lifetimes and lower quantum efficiencies than the corresponding Eu–TTASi–O–Si–O–M hybrids. This further verifies that the molecular linkage from single modification is more beneficial for the luminescence of the final hybrids.

Conclusions

A series of luminescent organic–inorganic hybrids based on the composite xerogels of silica and titanium/boron networks [Si–O–B(Ti)] with the β-diketone-functionalized linkages (TASi, TTASi, TTASi′) were obtained. These materials are homogeneous and no phase separation occurs, which is due to the formation of the Si–O–Si/Ti/B composite xerogels during the hydrolysis and polycondensation reactions between the β-diketone polysilsesquioxane bridge and tetraethyl orthosilicate/titanium butoxide/tributyl borate. The photoluminescence properties of these hybrids were studied and discussed in detail in terms of quantum efficiency, lifetimes, and red/orange intensity ratios. Firstly, the hybrids with the TTASi linkage show better photoluminescence performance than that with TASi, as TTASi is a better linkage (molecular bridge) for Eu^{3+}. Secondly, the hybrids with the single-modified TTA linkage (TTASi) present better luminescence than those with the double-modified TTA linkage (TTASi′), which suggests that single substitution is favorable for the luminescence of Eu^{3+}. Thirdly, is the most important, the hybrids of composite xerogels (Si–O–B) exhibit comparable luminescence behavior to the hybrids of pure Si–O xerogels, and both these exhibit a much more superior luminescence behavior than the hybrids of Si–O–Ti xerogels. This reveals that the hybrids based on Si–O–B xerogels will be promising candidates in many fields of applications. The mechanism of how these different host matrixes affect the luminescence properties in such hybrids needs further deep investigation.

Experimental Section

Materials: Thenoyltrifluoroacetylacetone (TTA) and trifluoroacetylacetone (TA) was purchased from Shanghai Chemical Plant, and 3-(triethoxysilyl)propyl isocyanate (TEPIC) was obtained from the Lancaster Company. Tetraethyl orthosilicate, titanium butoxide, and tributyl borate were available commercially and used without purification. The solvents (THF, DMF) used were purified by common methods. Europium nitrate was obtained from the corresponding oxide in concentrated nitric acid. Other starting (e.g. NaH) reagents were used as received.

Synthesis of Precursors and Materials: The precursor TASi, TTASi, and TTASi′ were prepared according to a known procedure[32] and characterized by ^1H NMR and FTIR spectroscopy. Here, we only give TTA as an example: TTA (1.0 mmol) was dissolved in anhydrous tetrahydrofuran (20 mL) with stirring, followed by addition of NaH (2 mmol, 0.08 g). After 2 h, TEPIC (1.2 mmol/0.28 g, 2.5 mmol/0.56 g) was added dropwise into the solution; the reaction lasted for 8 h. The whole mixture was heated at reflux at 65 °C, and all synthetic manipulations were performed under an atmosphere of argon in a three-necked bottle containing a magnetic stirrer. Finally, after isolation and purification, a yellow oily liquid product was obtained.

TASi: (M_w: 401.28, yield: 0.23 g, 57%). $C_{15}H_{26}F_3NO_6Si$ (401.45): calcd. C 44.90, H 6.48, N 3.49; found C 46.15, H 6.22, N 3.25. ^1H NMR: δ = 1.89 (s, 3 H, CH_3), δ = 5.39 (s, 1 H, CH), δ = 2.29 (m, 1 H, NH), δ = 3.1 (m, J = 6.8 Hz, 2 H, CH_2), δ = 0.61 (t, J = 8.4 Hz, 2 H, CH_2), δ = 3.80 (m, J = 7.2 Hz, 6 H, CH_2), δ = 1.19 (t, J = 6.8 Hz, 9 H, CH_3) ppm.

TTASi: (M_w: 468.54, yield: 0.29 g, 62%). $C_{18}H_{26}F_3NO_6SSi$ (469.55): calcd. C 46.07, H 5.54, N 2.98; found C 46.20, H 5.23, N 2.81. ^1H NMR: δ = 7.58 (d, 3.8 Hz, 2 H), δ = 6.9 (t, J = 5.0 Hz, 2

H), δ = 7.35 (d, J = 4.6 Hz, 2 H), δ = 2.27 (m, 1 H, NH), δ = 3.13 (m, J = 6.8 Hz, 2 H, CH_2), δ = 0.62 (t, J = 8.2 Hz, 2 H, CH_2), δ = 3.76 (m, J = 7.2 Hz, 6 H, CH_2), δ = 1.25 (t, J = 8.6 Hz, 9 H, CH_3) ppm.

TTASi′: (M_w: 714.9, yield: 0.43 g, 61%). $C_{25}H_{47}F_3N_2O_{10}Si_2$ (648.82): calcd. C 46.94, H 6.56, N 3.91; found C 47.12, H 6.36, N 3.77. ^{1}H NMR: δ = 7.50 (d, 3.6 Hz, 2 H), δ = 6.94 (t, J = 4.8 Hz, 2 H), δ = 7.31 (d, J = 4.8 Hz, 2 H), δ = 2.21 (m, 2 H, NH), δ = 3.12 (m, J = 6.8 Hz, 4 H, CH_2), δ = 0.6 (t, J = 8.4 Hz, 4 H, CH_2), δ = 3.78 (m, J = 7.2 Hz, 12 H, CH_2), δ = 1.20 (t, J = 8.8 Hz, 18 H, CH_3) ppm.

The eventual hybrid materials were prepared as follows: an appropriate amount of TTASi (TASi, TTASi′) was introduced into *N*,*N*-dimethyl formamide (DMF) with stirring. A stoichiometric amount of $Eu(NO_3)_3{\cdot}6H_2O$ was then added to the solution. After 2 h, a corresponding amount of tetraethyl orthosilicate was added, and the mixture was then stirred for 8 h vigorously at room temperature to obtain a single phase, which was transferred to an 80 °C oven for 5 d. The product was then removed and ground into a powder that was used for optical characterization studies. The mol ratio of $Eu(NO_3)_3{\cdot}6H_2O$/TTASi (TASi, TTASi′)/TEOS/H_2O is 1:3:12:48. Using the same method, we synthesized hybrids with the Si–O–B composite host by employing tributyl borate instead of tetraethyl orthosilicate. Titanium butoxide replaced tetraethyl orthosilicate in the preparation of the hybrids with the Si–O–Ti composite host. However, after titanium butoxide was added, the polycondensation reaction could not take place evenly because of the much faster hydrolysis rate of titanium butoxide. Therefore, it is important that it be added by drops in batches. The detailed synthetic procedure and the possible structure predicted of the hybrid materials are shown in Figure 1.

Measurements: ^{1}H NMR spectra were recorded in $CDCl_3$ on a BRUKER AVANCE-500 spectrometer with tetramethylsilane (TMS) as internal reference. FTIR spectra were obtained within the 4000–400 cm^{-1} region on an infrared spectrophotometer with the KBr pellet technique. The ultraviolet absorption spectra (using chloroform as solvent) were taken with an Agilent 8453 spectrophotometer. The UV/Vis diffuse reflectance spectra were acquired by a BWS003 spectrophotometer. The X-ray powder diffraction patterns were recorded on a Bruker D8 diffractometer (40 mA, 40 kV) by using monochromated Cu-$K_{\alpha 1}$ radiation (1.54 Å) over the 2θ range 10–70°. Thermogravimetric (TGA) curves were measured with a Netzsch instrument, model STA 409C, under nitrogen atmosphere in Al_2O_3 crucibles at a rate of 10 °C/min from 30 to 1000 °C. The luminescence excitation and emission spectra were obtained on a RF-5301 spectrophotometer. Luminescence lifetime measurements were carried out on an Edinburgh FLS920 phosphorimeter by using a 450-W xenon lamp as the excitation source. The microstructures were checked by scanning electronic microscopy (Philips XL30).

Supporting Information (see footnote on the first page of this article): Scheme of the synthesis process of the hybrids with TASi and TTASi′ linkages, FTIR spectra of the linkages, selected UV/Vis absorption spectra of TTASi′ and the hybrids, X-ray diffraction patterns of the hybrids with TASi and TTASi, and UV/Vis diffuse reflection absorption spectra of the hybrid materials.

Acknowledgments

This work is supported by the National Natural Science Foundation of China (20971100) and the Program for New Century Excellent Talents in University (NCET-08–0398).

[1] G. Blasse, *J. Solid State Chem.* **1998**, *72*, 72–79; T. Gunnlaugsson, J. P. Leonard, *Chem. Commun.* **2003**, *19*, 2424–2425; N. Sabbatini, A. Mecati, M. Guardigli, V. Balzani, J. M. Lehn, R. Zeissel, R. Ungaro, *J. Lumin.* **1991**, *48–9*, 463–468; M. Elbanowski, B. Makowsaka, *J. Photochem. Photobiol. A: Chem.* **1996**, *99*, 85–92.

[2] S. I. Weissman, *J. Chem. Phys.* **1942**, *10*, 214–217.

[3] C. M. G. dos Santos, P. B. Fernandez, S. E. Plush, J. P. Leonard, T. Gunnlaugsson, *Chem. Commun.* **2007**, 3389–3391; J. C. G. Bunzli, C. Piguet, *Chem. Rev.* **2002**, *102*, 1897–1928; J. Kido, Y. Okamoto, *Chem. Rev.* **2002**, *102*, 2357–2368.

[4] T. Jin, S. Tsutsumi, Y. Deguchi, K. I. Machida, G. Y. Adachi, *J. Electrochem. Soc.* **1995**, *142*, L195–L197.

[5] P. N. Minoofar, R. Hernandez, S. Chia, B. Dunn, J. I. Zink, A. C. Franville, *J. Am. Chem. Soc.* **2002**, *124*, 14388–14396; L. Zhao, M. Vaupel, D. A. Loy, K. J. Shea, *Chem. Mater.* **2008**, *20*, 1870–1876; J. A. Chaker, C. V. Santilli, S. H. Pulcinelli, K. Dahmouche, V. Briois, P. Judeinstein, *J. Mater. Chem.* **2007**, *17*, 744–757.

[6] T. Suratwala, Z. Gardlund, K. Davidson, D. R. Uhlmann, J. Watson, N. Peyghambarian, *Chem. Mater.* **1998**, *10*, 190–198; T. Suratwala, Z. Gardlund, K. Davidson, D. R. Uhlmann, J. Watson, S. Bonilla, N. Peyghambarian, *Chem. Mater.* **1998**, *10*, 199–209; C. Molina, K. Dahmouche, C. V. Santilli, A. F. Craievich, S. J. L. Ribeiro, *Chem. Mater.* **2001**, *13*, 2818–2823.

[7] A. C. Franville, D. Zambon, R. Mahiou, Y. Troin, *Chem. Mater.* **2000**, *12*, 428–435; F. Embert, A. Mehdi, C. Reye, R. J. P. Corriu, *Chem. Mater.* **2001**, *13*, 4542–4549; H. R. Li, J. B. Yu, F. Y. Liu, H. J. Zhang, L. S. Fu, Q. G. Meng, C. Y. Peng, J. Lin, *New J. Chem.* **2004**, *28*, 1137–1141; P. P. Lima, R. A. S. Ferreira, R. O. Freire, F. A. A. Paz, L. S. Fu, S. Alves, L. D. Carlos, O. L. Malta, *ChemPhysChem* **2006**, *7*, 735–746; P. Lenaerts, A. Storms, J. Mullens, J. D′Haen, C. Gorller-Walrand, K. Binnemans, K. Driesen, *Chem. Mater.* **2005**, *17*, 5194–5201.

[8] C. Y. Yang, V. Srdanov, M. R. Robinson, G. C. Bazan, A. J. Heeger, *Adv. Mater.* **2002**, *14*, 980–983; X. F. Qiao, B. Yan, *Dalton Trans.* **2009**, *40*, 8509–8518; X. F. Qiao, B. Yan, *Inorg. Chem.* **2009**, *48*, 4714–4723.

[9] K. Lunstroot, L. Baeten, P. Nockemann, J. Martens, P. Verlooy, X. P. Ye, C. Gorller-Walrand, *J. Phys. Chem. C* **2009**, *113*, 13532–13538; K. Lunstroot, K. Driesen, P. Nockemann, C. Gorller-Walrand, K. Binnemans, S. Bellayer, J. Le Bideau, A. Vioux, *Chem. Mater.* **2006**, *18*, 5711–5715; S. Arenz, A. Babai, K. Binnemans, K. Driesen, R. Giernoth, A. V. Mudring, P. Nockemann, *Chem. Phys. Lett.* **2005**, *402*, 75–79; K. Binnemans, C. Gorller-Walrand, *Chem. Rev.* **2002**, *102*, 2303–2345.

[10] P. Escribano, B. Julian-Lopez, J. Planelles-Arago, E. Cordoncillo, B. Viana, C. Sanchez, *J. Mater. Chem.* **2008**, *18*, 23–40; C. Sanchez, B. Julian, P. Belleville, M. Popall, *J. Mater. Chem.* **2005**, *15*, 3559–3592; C. Sanchez, G. J. D. A. Soler-Illia, F. Ribot, T. Lalot, C. R. Mayer, V. Cabuil, *Chem. Mater.* **2001**, *13*, 3061–3083.

[11] L. N. Sun, H. J. Zhang, L. S. Fu, F. Y. Liu, Q. G. Meng, C. Y. Peng, J. B. Yu, *Adv. Funct. Mater.* **2005**, *15*, 1041–1048.

[12] H. R. Li, J. Lin, H. J. Zhang, H. C. Li, L. S. Fu, Q. G. Meng, *Chem. Commun.* **2001**, *13*, 1212–1213; N. N. Lin, H. R. Li, Y. G. Wang, Y. Feng, D. S. Qin, Q. Y. Gan, S. D. Chen, *Eur. J. Inorg. Chem.* **2008**, *30*, 4781–4785.

[13] P. Lenaerts, A. Storms, J. Mullens, J. D′Haen, C. Gorller-Walrand, K. Binnemans, K. Driesen, *Chem. Mater.* **2005**, *17*, 5194–5201.

[14] L. D. Carlos, R. A. S. Ferreira, V. D. Bermudez, S. J. L. Ribeiro, *Adv. Mater.* **2009**, *21*, 509–534; K. Binnemans, *Chem. Rev.* **2009**, *109*, 4283–4374.

[15] Q. M. Wang, B. Yan, *J. Mater. Chem.* **2004**, *14*, 2450–2455; Q. M. Wang, B. Yan, *Cryst. Growth Des.* **2006**, *5*, 497–503; J. L. Liu, B. Yan, *J. Phys. Chem. B* **2008**, *112*, 10898–10907; H. F. Lu, B. Yan, J. L. Liu, *Inorg. Chem.* **2009**, *48*, 3966–3975; L. Guo, B. Yan, *Eur. J. Inorg. Chem.* **2010**, 1267–1274.

[16] Y. Li, B. Yan, H. Yang, *J. Phys. Chem. C* **2008**, *112*, 3959–3968; B. Yan, Y. Li, B. Zhou, *Microporous Mesoporous Mater.* **2009**, *120*, 317–324; Y. Li, B. Yan, *Microporous Mesoporous Mater.* **2010**, *128*, 62–70; Y. Li, B. Yan, Y. J. Li, *Microporous Mesoporous Mater.* **2010**, *132*, 87–93; Y. J. Li, B. Yan, Y. Li, *Chem. Asian J.* **2010**, *5*, 1642–1651.
[17] B. Yan, X. F. Qiao, *J. Phys. Chem. B* **2007**, *111*, 12362–12374; X. F. Qiao, B. Yan, *J. Phys. Chem. B* **2008**, *112*, 14742–14750; X. F. Qiao, B. Yan, *J. Phys. Chem. B* **2009**, *113*, 11865–11875; K. Sheng, B. Yan, L. Guo, J. L. Liu, *Eur. J. Inorg. Chem.* **2010**, 3498–3475.
[18] B. Yan, Q. M. Wang, *Cryst. Growth Des.* **2008**, *8*, 1484–1489; L. Guo, B. Yan, *Inorg. Chem. Commun.* **2010**, *13*, 358–360; B. Yan, C. Wang, L. Guo, J. L. Liu, *Photochem. Photobiol.* **2010**, *86*, 499–506.
[19] M. Gratzel, *Nature* **2001**, *414*, 338–344; P. Wang, C. Klein, R. Humphry-Baker, S. M. Zakeeruddin, M. Gratzel, *J. Am. Chem. Soc.* **2005**, *127*, 808–809; M. H. Bartl, S. W. Boettcher, K. L. Frindell, G. D. Stucky, *Acc. Chem. Res.* **2005**, *38*, 263–271.
[20] N. J. Turro, *Modern Molecular Photochemistry*, University Science Books, **1991**.
[21] M. C. Goncalves, V. D. Bermudez, R. A. S. Ferreira, L. D. Carlos, D. Ostrovskii, J. Rocha, *Chem. Mater.* **2004**, *16*, 2530–2543.
[22] E. Pretsch, P. Buhlmann, C. Affolter (Eds.), *Structure Determination of Organic Compounds*, 2nd ed., Springer: Berlin, **2003**.
[23] K. Nakamoto, *Infrared and Raman Spectra of Inorganic and Coordination Compounds, Part A Theory and Applications in Inorganic Chemistry*, 6th ed., Wiley-Interscience, **2009**.
[24] K. S. Guan, Y. S. Yin, *Mater. Chem. Phys.* **2005**, *92*, 10–15.
[25] H. R. Li, J. Lin, H. J. Zhang, L. S. Fu, Q. G. Meng, S. B. Wang, *Chem. Mater.* **2002**, *14*, 3651–3655.
[26] B. J. Gao, Y. F. Yang, Y. Cheng, D. J. Shi, *Spectrosc. Spectrosc. Anal.* **2002**, *22*, 371–374.
[27] D. L. J. Dexter, *J. Chem. Phys.* **1953**, *21*, 836–850.
[28] M. Nogami, Y. Moriya, *J. Non-Cryst. Solids* **1982**, *48*, 359–366.
[29] Y. Hasegawa, M. Yamamuro, Y. Wada, N. Kanehisa, Y. Kai, S. Yanagida, *J. Phys. Chem. A* **2003**, *107*, 1697–1702.
[30] E. E. S. Teotonio, J. G. P. Espinola, H. F. Brito, O. L. Malta, S. F. Oliveria, D. L. A. de Faria, C. M. S. Izumi, *Polyhedron* **2002**, *21*, 1837–1844; M. H. V. Werts, R. T. F. Jukes, J. W. Verhoeven, *Phys. Chem. Chem. Phys.* **2002**, *4*, 1542–1548; P. C. R. Soares-Santos, H. I. S. Nogueira, V. Felix, M. G. B. Drew, R. A. S. Ferreira, L. D. Carlos, T. Trindade, *Chem. Mater.* **2003**, *15*, 100–108.
[31] J. C. Boyer, F. Vetrone, J. A. Capobianco, A. Speghini, M. Bettinelli, *J. Phys. Chem. B* **2004**, *108*, 20137–20143; L. D. Carlos, Y. Messaddeq, H. F. Brito, R. A. S. Ferreira, V. D. Bermudez, S. J. L. Ribeiro, *Adv. Mater.* **2000**, *12*, 594–598.
[32] B. Yan, L. L. Kong, B. Zhou, *J. Non-Cryst. Solids* **2009**, *355*, 1281–1284; B. Yan, Y. Li, *Dalton Trans.* **2010**, *39*, 1480–1487.

Received: October 8, 2010
Published Online: January 20, 2011

